**Atmospheric
Chemistry
and Physics
Discussions**

Mesoscale
circulations over
complex terrain:
meteorology

G. Pérez-Landa et al.

Mesoscale circulations over complex terrain in the Valencia coastal region, Spain, Part 1: simulation of diurnal circulation regimes

G. Pérez-Landa[1], P. Ciais[2], M. J. Sanz[1], B. Gioli[3], F. Miglietta[3], J. L. Palau[1], G. Gangoiti[4], and M. M. Millán[1]

[1]Fundación CEAM. Parque Tecnológico, c/ Charles R. Darwin 14, 46980 Paterna (Valencia), Spain
[2]Laboratoire des Sciences du Climat et de l'Environnement, UMR Commissariat à l'Energie Atomique/CNRS 1572, Gif-sur-Yvette, France
[3]IBIMET-CNR, Instituto di Biometeorologia, Consiglio Nazionale delle Ricerche, Firenze, Italy
[4]Escuela Técnica Superior de Ingenieros Industriales de Bilbao, Universidad del País Vasco/Euskal Herriko Unibertsitatea, Bilbao, Spain

Correspondence to: G. Perez-Landa (gorkapl@confluencia.biz)

Title Page

Abstract	Introduction
Conclusions	References
Tables	Figures

|◄ | ►|

◄ | ►

Back | Close

Full Screen / Esc

Printer-friendly Version

Interactive Discussion

EGU

Mesoscale circulations over complex terrain: meteorology

G. Pérez-Landa et al.

Full Screen / Esc

Printer-friendly Version

Interactive Discussion

EGU

Abstract

We collected ground-based and aircraft data on meteorological parameters and CO_2 fluxes and concentrations during a 2-week intensive campaign over the Valencia basin, as part of a process study to understand how mesoscale circulations over complex

5 terrain develop and affect the atmospheric transport acting on surface CO_2 fluxes. In this paper, we interpret the meteorological data during a selected case, with the help of a very high resolution mesoscale model to understand the diurnal cycle of mesoscale flow regimes, characterized by night-time katabatic drainage, morning sea-breeze development and subsequent coupling with mountain up-slopes, and evening

10 flow-veering under larger-scale influences. At each step, a careful statistical analysis of the model performances is carried out. Despite the inherent complexity of the processes interacting with each other, and large model uncertainties for soil moisture boundary conditions and turbulence parameterizations, we show that it is possible to simulate faithfully the flow regimes, especially the inland progression and organization

15 of the sea breeze. This provides confidence with respect to the future applicability of mesoscale models to establish a missing link between surface sources of CO_2 and atmospheric concentration signals over complex terrain.

1 Introduction

More than 75% of the Earth's population lives within 60 km of the sea (Michener at al.,

20 1997), and many coastal cities are surrounded by hills or mountains. Many anthropogenic emissions of CO_2 and pollutants are thus located in coastal regions, where complex terrain mesoscale circulations are likely to inject the sources signal into the atmosphere with very specific patterns. These patterns are not resolved in coarse-scale global transport models, and deserve new process studies to better understand how

25 the atmospheric integrator operates at small scales. Solar heating frequently creates thermally induced mesoscale circulations that develop under clear sky conditions, with

strong diurnal variations, and with patterns and intensities that depend on the regional surface energy budget and the orography. The formation and transport of pollutant layers has been related to these mesoscale circulations, in particular to the interaction between the sea breeze and mountain circulations at the coastal regions. This process

5 has been observed at Athens (Lalas et al., 1987), Los Angeles (Lu and Turco, 1994), British Columbia (McKendry et al., 1997), Tokyo (Chang et al., 1989), and over the Northern (Millán et al., 1984) and Eastern (Millán et al., 1992) coasts of Spain.

The Western Mediterranean Basin is surrounded by high mountains and during summer clear-sky conditions prevail. In total, 42 million people live in urban areas on the

10 Western Mediterranean coast (Attane and Courbage, 2004). Former campaigns have shown that mesoscale processes dominate the meteorological regimes of that region (Millán et al., 1997). Regional circulations present a marked diurnal cycle and become self-organized from cells of tenths of kilometers in the early stages of the cycle, to circulations extending to the whole basin (hundreds of kilometers) later in the evening

15 (Gangoiti et al., 2001). The presence of stacked layers of pollutants has been identified as a result of the recirculation of airmasses in the Mediterranean basin, driven by mesoscale transport (Millán et al., 1992; Millán et al., 1997). In the latter study, ozone was considered as a tracer of the polluted air-masses, characterized by aircraft vertical profiles and surface measurements, and interpreted with the help of mesoscale mod-

20 els. Additionally, the coupling between mesoscale model simulations and a Lagrangian particle dispersion model was found useful in the description of transport patterns in the region under such conditions (Gangoiti et al., 2001; Pérez-Landa et al., 2002).

Ozone and reactive gases or aerosols present limitations as tracers of mesoscale transport, given their active sources and sinks in the atmosphere. Passive tracers can

25 be released artificially and their measured concentrations used to validate transport (Moran and Pielke, 1996), but these tracer release experiments are sporadic, expensive, and limited to point sources. Carbon dioxide (CO_2) can potentially be used as a very valuable transport tracer; it is a passive tracer, relatively easy to measure, and emitted by nearly all land and ocean surfaces, including anthropogenic sources. Nev-

ertheless, there are some specific difficulties complicating the use of CO_2 as an ideal tracer of transport over complex terrain. First, one must know the magnitude of the CO_2 surface fluxes, otherwise the concentration signals cannot be unambiguously related to transport alone (in fact, in carbon cycle studies, the problem is reversed and scientists attempt to determine unknown CO_2 sources and sinks, assuming known large-scale transport). Second, the diurnal cycle of land biotic CO_2 fluxes (respiration source at night and photosynthesis sink during the day) is coupled with the diurnal cycle of transport processes, which induces "rectification" effects (Denning et al., 1995). Over flat terrain, rectification effects with nighttime built up of respired CO_2 sources near the surface and daytime dilution of CO_2 sinks by convective mixing, shape the vertical profiles of CO_2 (Wofsy et al., 1998; Balkwin et al., 1998; Chevillard et al., 2002). Over complex terrain, one can anticipate that diurnal mesoscale circulations control both the vertical and the horizontal CO_2 gradients.

At the regional scale, aircraft measurements have already proved useful, providing information about CO_2 spatial and temporal patterns (Crawford et al., 1996; Desjardins et al., 1982, 1997; Gioli et al., 2004; Ritter et al., 1994). In this study, we use CO_2 concentration measurements from a campaign over complex terrain to gain knowledge on the coupling of mesoscale transport processes and rectification effects. Emphasis is placed on the acquisition and interpretation of horizontal wind and CO_2 profiles to constrain the small-scale transport processes, in particular the formation of layers with distinct CO_2 signatures. In order to use CO_2 as a quantitative tracer of mesoscale transport, the surface fluxes are independently constrained by continuous eddy-covariance measurements and by airborne flux measurements during the campaign.

The campaign was carried out in June 2001 in the Valencia region, a coastal basin with complex terrain located on the East coast of Spain, as part of the RECAB project (Regional Assessment and Modelling of the Carbon Balance in Europe). Airborne measurements and ground-based continuous observations of CO_2 fluxes and meteorological variables were collected during the two weeks of the campaign (Gioli et al., 2004). During most days of the campaign, vertical profiling of the lower atmosphere showed

a complex structure of the CO_2 mixing ratio, with large vertical gradients changing with time. Interpretation of these data must be done in terms of the coupling between diurnal cycles of biological fluxes and mesoscale processes.

Mesoscale meteorological models have proved to be important tools for helping to understand the temporal and spatial variation of CO_2 mixing ratios in the atmosphere at the regional scale (Nicholls et al., 2003; Chevillard et al., 2002; Eastman et al., 2001). In this study we attempt to quantify the influence of mesoscale processes and their coupling with biological phenomena, causing spatial and temporal CO_2 variability in the region of Valencia. A high-resolution mesoscale meteorological model is coupled to a Lagrangian particle dispersion model allowing the transport simulation of CO_2 over the Valencia region. In this first paper, we present the experimental and modeling set-up and the simulated meteorological fields with the purpose of describing the main meteorological processes responsible for mesoscale transport of CO_2. In a companion paper (this issue) we make the link between surface CO_2 fluxes and observed CO_2 concentrations by calculating CO_2 transport simulations with a Lagrangian particle dispersion model.

The following sections describe summertime conditions for mesoscale transport processes in the Western Mediterranean area (Sect. 2), the RECAB campaign experimental results (Sect. 3) and modeling simulations (Sect. 4). The model results are evaluated in detail against observations (Sect. 5), and discussed in light of air masses recirculation and breeze effects (Sect. 6).

2 Campaign design implied by regional and local conditions

2.1 Relevant features at local and regional scales

The orography of the Western Mediterranean Basin (WMB) exerts a strong influence on its weather regimes, generating local and regional mesoscale circulations on diurnal time scales (Millán et al., 1997, 2002; Gangoiti et al., 2001). The main orographic

features are illustrated in Fig. 1a. In summer, a quasi-permanent thermal low-pressure system becomes established during the day over the Iberian Peninsula (Millán et al., 1996). This so-called Iberian Thermal Low (ITL) is driven by the convergence of different circulation cells, with the merging of different up-slope winds and sea-breezes developed from coastal areas. On the coast, sea breezes combine with up-slope winds to transport wet air inland. In the interior, at the front of the combined breeze, the wet air can be injected into a return flow at typical heights of 2–3 km (Millán et al., 1997). During the day, the development of the ITL and the resulting generalized convergence of wind at ground level along the coast are compensated by an increased subsidence over the Mediterranean Sea and the Atlantic (Millán et al., 1997). During the night, all these processes relax and gravity flows dominate along the valleys open to the sea (Millán et al., 1992). This creates a nocturnal divergence of air near the surface, which is advected towards the sea. This suite of processes is characterized by a marked diurnal cycle of the wind flow and pressure. It allows a recirculation of air masses with a periodicity of at least 3 days, as shown by tracer experiment results (Millán et al., 1992). Such mesoscale circulations develop coherently at a scale that may encompass the whole WMB (Millán et al., 1997; Gangoiti et al., 2001). Thus, it is necessary to consider mesoscale circulations around the WMB as a whole, in order to properly quantify and understand the transport of CO_2 over a small region, here the Valencia basin. In this respect, it should be remembered that similar mesoscale processes involving either vertical re-circulations and/or oscillations were found in the Central Mediterranean (Georgiadis et al., 1994; Orciari et al., 1998) and in the Eastern Mediterranean basins (Kallos et al., 1997; Ziomas et al., 1998).

The Valencia region is located on the East coast of the Iberian Peninsula. At the confluence of the Turia (North) and Jucar (South) river basins, the region presents a coastal plain extending up to 50 km inland (Fig. 1b), surrounded by mountain ranges with an average elevation of 1000 m. The Valencia plain's combination of proximity to the sea, mild temperatures and flat topography allows large-scale cultivation of irrigated tree-crops (mainly citrus) and paddy rice next to the coast. The city of Valencia located

Mesoscale circulations over complex terrain: meteorology

G. Pérez-Landa et al.

Title Page

Abstract | Introduction

Conclusions | References

Tables | Figures

◄ | ►

◄ | ►

Back | Close

Full Screen / Esc

Printer-friendly Version

Interactive Discussion

EGU

at the mouth of the Turia river (Fig. 1b) is a medium-size city of 1.4 M people, including conurbations, with no heavy industry.

2.2 Mediterranean region conditions during the early summer 2001

The monthly averaged Sea Level Pressure and 2-m temperature fields in June 2001 are shown in Fig. 2a. Data are six-hourly meteorological re-analyses provided by the European Center for Medium-Range Weather Forecasts (ECMWF) at ∼50 km spatial resolution (Simons et al., 2000). The temperature field shows a pronounced heating in the southern continental areas, with a strong gradient between the North and the South of the Iberian Peninsula. The Sea Level Pressure map shows the Azores High extended over the Bay of Biscay towards the European continent at the western edge of the domain, the Asian Monsoon system at the Eastern edge of the domain, and the low-pressure belt of the Inter-Tropical Convergence Zone south of the Atlas Mountains in Africa (Fig. 2a). The Sea Level Pressure decreases eastwards from maximum values over the Atlantic coast to minimum values over the Arabian Peninsula. Such features are representative of summer conditions, and were already noticed in previous studies (Millán et al., 1997; Gangoiti et al., 2001). The current spatial resolution of the ECMWF model is too coarse to resolve regional mesoscale circulations well, but hints of these circulations can be seen in Fig. 2a. There is for instance a ring of low pressure over the Iberian and Anatolian peninsulas, suggesting the existence of local thermal lows. The average diurnal cycle of Sea Level Pressure, taken from the difference between 06:00 and 18:00 UTC, is shown in Fig. 2b. It confirms the existence of a thermally induced decrease in pressure in the interior of continents, with minimum values during the evening. Over the main valleys of the Iberian Peninsula, the amplitude of the diurnal pressure cycle is higher than 3.5 mb, while over Anatolia, it is lower than 3.5 mb. The strongest diurnal pressure variations (>4.5 mb) are visible over Northern Africa. It is likely that the diurnal pressure variation would be even higher in a model with a finer grid than the ECMWF one, and thus better at resolving orography and its associated circulations.

Mesoscale circulations over complex terrain: meteorology

G. Pérez-Landa et al.

Title Page

Abstract	Introduction
Conclusions	References
Tables	Figures

◄ | ►

◄ | ►

Back | Close

Full Screen / Esc

Printer-friendly Version

Interactive Discussion

EGU

2.3 Valencia region conditions during the campaign

From a synoptic analysis of twenty years of weather maps, we determined that the period of maximum occurrence of the ITL lies between 23 June and 20 August. During this interval, daytime thermal low-pressure systems develop inland an average of more than 70% of the days (Hutjes et al., 2003). In the meantime, the period of highest vegetation activity in the Valencia region lasts from April to June, before soil drying causes photosynthesis to drop during the peak of summer (Miglietta et al., 2001). We sought to carry out the campaign at a time when both typical well-developed sea breeze conditions contributing to the ITL and active vegetation CO_2 fluxes could coexist. Consequently, we selected an early summertime window from 20 June to 5 July 2001, with an intensive observation period carried out on 2 July (see Sect. 3).

Inspection of the synoptic charts for the campaign period shows that during the two-week campaign, the Iberian Peninsula was influenced by a high pressure system centered over the Netherlands, spreading towards Central Europe and the WMB. A low pressure system was centered West of Ireland, but its influence did not reach the Iberian Peninsula until 4 July, with the exception of a very weak trough crossing the peninsula from West to East on 27 June. For the remaining days of the campaign, the skies were sunny and cloudless, favoring the development of the ITL. Thus, according to the previously mentioned studies, during the campaign a marked diurnal cycle of winds in the Valencia region could be expected due to the development of the mentioned mesoscale circulations. Note also that, under these conditions, the region is quite typical of the whole WMB, so these findings from the RECAB study could be generalized to other Mediterranean coastal areas with similar features.

3 Airborne and ground-based measurements during the campaign

We focus here on 2 July, during which many successive vertical profiles were collected over the rice fields near the coastline (Fig. 1a). The weather conditions for this day

show a high pressure system centered over the Netherlands and southern UK and the typical sea level pressure decrease towards the East in the Mediterranean region (Fig. A1). There is a local pressure minimum over the center of the Iberian Peninsula at 12:00 UTC, where the temperature is locally warm at that time. Thus, under this weather pattern, development of the previously discussed mesoscale processes is expected in the region of interest.

The main measurements made on 2 July consist of airborne vertical profiles and horizontal transect measurements of CO_2 concentrations and meteorological variables, at successive intervals of about 3 h (Table 1). The aircraft routes are shown in Fig. 1b. The Sky Arrow ERA airplane can measure concentrations and fluxes, the latter by eddy-covariance technique. Measurements of sensible and latent heat fluxes (CO_2 fluxes are in the companion paper) and of meteorological parameters (temperature, relative humidity and wind) are described by Gioli et al. (2004). Vertical profiles were collected between 15 m and 800 m height over the rice fields. Airborne flux measurements were performed along each horizontal transect shown in Fig. 1b.

Airborne observations are supplemented by collocated ground-based eddy covariance flux measurements. Fluxes of CO_2, H_2O and energy were measured on top of two towers (Fig. 1b) by the eddy-covariance technique. The first flux tower (12 m), called El Saler (SA), is permanently located over a Pine-dominated maquia forest. The second tower (2 m), called Rice (RI), was set up during the campaign over a rice field. Eddy covariance fluxes of sensible and latent heat (CO_2 fluxes are part of the companion paper) are calculated at 30 min time steps from ultrasonic anemometer wind, H_2O and temperature sensors 10 Hz data, following the guidelines of the standard Euroflux methodology (Aubinet et al., 2000). Ancillary measurements of wind speed and direction, temperature and relative humidity are also performed on top of each flux tower and will be used to evaluate the simulated meteorology (Sect. 5). In addition to the two coastal meteorological stations at the flux tower locations, we also collected measurements from stations located further inland within the Valencia basin, Villar (VI) and Xátiva (XA), and from three additional stations North of the city of Valencia, Altura (AL),

Port (PO) and Carraixet (CA). Thus, in total, we analyzed data from 7 different stations, which enabled us to characterize the temperature and wind regime within the region of interest.

4 Mesoscale simulation: Model setup, initial and boundary conditions

The Regional Atmospheric Modeling System (RAMS; Pielke et al., 1992) in its version 4.3.0 was used to simulate selected days of the RECAB campaign. The RAMS model was applied for four domains of decreasing size at increasing spatial resolution (Fig. 1a). Our version of the RAMS model includes the TKE level 2.5 parameterization of turbulence (Mellor and Yamada, 1982), a full-column two-stream single-band radiation scheme that accounts for clouds for calculating short-wave and long-wave radiation (Chen and Cotton, 1983), and Kuo-modified parameterization of sub-grid scale convection processes in the coarse domain (Molinari, 1985). The cloud and precipitation microphysics scheme of Walko et al. (1995) was applied in all the domains. The LEAF-2 soil-vegetation surface scheme was used to calculate sensible and latent heat fluxes exchanged with the atmosphere, using prognostic equations for soil moisture and temperature (Walko et al., 2000).

Several tests performed with the terrain processor of the model and different grid spacing, showed that in order to reproduce the orographic features of the Valencia basin (Fig. 1b), it is necessary to use a horizontal resolution as high as 1–2 km. This is coherent with former studies which showed the need to use a grid size of at least 2 km to capture properly the terrain variance in this region (Salvador et al., 1999). A configuration of four two-way interactive nested domains was defined accordingly for RAMS, also compatible with the computing power available (Fig. 1a). The coarsest first domain covers the whole WMB, an area bounded by –19° W, 27° N and 16° E, 49° N, with 89×73 grid points with a length of 40.5 km. The second domain covers the Iberian Peninsula at 13.5 km grid spacing (125×95 grid cells). The third domain covers the Valencia region at a grid spacing of 4.5 km (83×83 grid cells), while the smallest inner

domain covers the Valencia basin and the campaign location at a grid spacing of 1.5 km (83×83 grid cells). The vertical discretization uses 45 levels with a 30 m spacing near the surface increasing gradually up to 1000 m near the model top at 17 000 m and with 15 levels in the lower 1000 m.

Boundary and initial conditions of atmospheric fields are derived from the analysis of the NCEP Aviation (AVN) run of the Global Spectral Model (Caplan et al., 1997), available every 6 h at ≈100 km resolution onto 42 vertical levels. A Four Dimensional Data Assimilation (FDDA) technique is applied in this study to define the forcing at the lateral boundaries of the outermost eight grid cells of the largest domain. Surface boundary conditions also include land cover maps. We use here the USGS land cover (Anderson et al., 1976) modified to include detailed land use information from CORINE (CEC, 1995) over the Iberian Peninsula, and from PELCOM (Mucher et al., 2000) over the rest of Europe. The various land cover types in each of the three databases are reclassified into the 30 distinct LEAF-2 vegetation classes with an original resolution of 0.0083° (Baklanov et al., 2004). Over the ocean, we prescribe SST values at 0.5° resolution from weekly means global data (Reynolds, 1994) combined with direct processing of NOAA-AVHRR raw satellite data during the days of the campaign following the scheme by Badenas et al. (1997).

The soil-moisture distribution plays a central role in the development of mesoscale circulations (Ookouchi et al., 1984; Lanicci et al., 1987; Jacobson 1999), with most of the difficulties consisting in the proper initialization of that variable. Soil moisture is usually estimated in global models, using atmospheric variables near the surface as forcing data (Mahfouf, 1991). Instead of this, we initialized soil moisture from the results of a "spin up" simulation of RAMS with LEAF-2 over the first two largest domains during the two months preceding the campaign. Thus, a simulation is started at 00:00 UTC on 1 May 2001. Namely, a smooth FDDA in the center of both domains is performed. The "clay-loam" soil type is subdivided into 11 layers down to the 2 m depth, with uniform initial soil moisture values of 0.38 m^3/m^3. The initial soil temperature profile is obtained by subtracting from the surface air temperature a value

Mesoscale circulations over complex terrain: meteorology

G. Pérez-Landa et al.

of 2.3°C in the top-soil, which linearly decreases down to a decrease of 1°C in the lowest soil level. Then, the simulated soil moisture and temperature calculated by the end of the two months' spin-up is interpolated to provide the initial conditions for the campaign over the four nested domains shown in Fig. 1a. This approach for deriving initial soil moisture by using modeled values alone does not take into account the observed precipitation or radiation data employed in other schemes (Smith et al., 1994), so that any bias in our coarse-resolution spin-up run may create unrealistic soil moisture conditions. Despite its simplicity, in this case our initialization procedure was found to provide better performances, when compared against atmospheric measurements, than if we had prescribed homogeneous values of soil water content such as in the default scheme proposed in RAMS 4.3.0. During the preparation of this manuscript, we became aware of a similar study over the Amazon region where nearly the same procedure was employed to initialize RAMS soil parameters (Lu et al., 2005).

5 Observed and simulated meteorology on 1 and 2 July 2001

5.1 Time series of temperature, humidity and wind

We describe here the time series from three stations, SA (El Saler, coastal), VI (Villar, inland in the Jucar river valley) and XA (Xàtiva, inland in the Turia river valley). Both inland stations show a larger diurnal temperature cycle (15°C) than the coastal station (8°C), as can be observed in Fig. 3. The model captures quite well the diurnal changes at each station (see statistical analysis in Sect. 6), as well as the gradient between the coastal station SA and the inland ones XA and VI. The warming trend observed at all three stations between 1 and 2 July, reaching up +5°C at XA, is well simulated. However, there is some noticeable under-prediction in the SA diurnal temperature cycle, of up to 3°C, showing overly high minimum and overly low maximum values.

The diurnal changes in relative humidity also show different amplitudes between inland and coastal stations. Inland sites VI and XA with RH values of less than 10%

by midday are strikingly dryer than coastal site SA, where RH varies in the range 30 to 50%. The model also shows good skills simulating relative humidity variations, although some shortcomings are apparent. At VI, it overestimates the relative humidity, especially during the night. In contrast, at SA, the model does a good job reproducing hourly changes in RH during the 2 July campaign, but it coarsely overestimates RH variations for 1 July. The moisture cycle at XA is well simulated on both days.

The hourly wind speed and direction are shown in Fig. 3. At all three stations, we can observe a strong diurnal oscillation in the wind regime, characterized by the daytime development of the sea-breeze advecting air from sea to land at a speed of up to 6 ms^{-1}, followed by the establishment of surface drainage winds oriented from land to sea.

During the daytime, thermal circulations develop, stabilizing a flow pattern which advects air from sea to land. The wind blows essentially inland from the East, but it is occasionally variable during the daytime and its direction is fairly site-dependent: at SA, we can observe winds blowing from the East first and then back to the North-East on the evening of 2 July (Fig. 3). In XA, the winds blow initially from the North-East, change to the North-West by the evening of 1 July, and finally to the South-West by the evening of 2 July. Thus, in spite of the proximity of the three stations, less than 100 km apart from each other, significant differences in wind direction can be observed and are related to orography and thermal forcing. This results are in good agreement with the mean wind field averaged at these stations during the last five years, indicative of their statistical significance (Appendix A).

During the night, the drainage winds follow the main axis of the local valleys (see Fig. 3). We can see nocturnal winds blowing from the South-West at XA along the Jucar valley (Fig. 3). At VI, calm conditions within a stable stratified surface layer prevail and consequently there is no representative wind direction. At SA, near the coast, the wind blows from the South-West during the night of 30 June–1 July, and from the North-West during the night of 1–2 July. The SA station is located at the confluence of the Jucar and Turia valleys (Fig. 1b) so that the main nocturnal wind

direction there can depend on which of the two drainage flows prevail (accordingly to the statistical features identified for this station during nighttime, Appendix A).

It is very encouraging to see that the model is able to capture quite realistically both the timing and the intensity of the drainage winds and breezes (Fig. 3). Yet, some dis-
5 crepancies with the station data are observed, especially during the night under stable conditions. At VI, the modeled wind speed and direction match the data during the day, except for the change late in the evening of 2 July (Fig. 3). At XA, the model predicts a change in wind direction from North-East to East by mid-day on 2 July, whereas the data show a variable wind direction. A second change in wind direction by the evening
10 of 2 July is simulated, with winds from the North, while the observed winds are from the South-West. At SA, on the coast, the daytime sea breeze development is well re-produced, especially during the 2 July campaign (Fig. 3). Regarding nocturnal flows, we found that at VI, the modeled drainage wind speed is overestimated by $1.5\,\mathrm{ms}^{-1}$, probably due to the presence of a ground inversion not resolved in the model, while at
15 XA and SA the modeled winds are occasionally in the wrong direction.

5.2   Comparison between aircraft observations and model simulation of wind field

The horizontal wind distribution at 50 m above ground-level measured during the air-craft transects is shown for early morning (Fig. 4a) and for mid-day (Fig. 4b) on 2 July. During the early morning, the drainage winds are flowing towards the sea. In the north-
20 ern basin (Turia), the wind speed is low and the wind comes from the North-West, while in the southern basin (Jucar), the wind turns to the West and increases its speed. At the confluence between the Jucar and Turia valleys, the wind acquires a different di-rection and speed. There is good agreement between model and data, except for an underestimation of the drainage winds in the southern basin (Fig. 4a). In contrast with
25 the early-morning complex wind field (driven by orography and gravity), by mid-day, the wind is more uniform and comes from the South-East, with higher speeds than during the morning on the coastal strip. This flow is nicely reproduced by the model, although a small deviation in wind direction is observed in the northern basin (Fig. 4b).

EGU

Figure 5 shows the profiles of horizontal wind acquired on 2 July onboard the Sky Arrow aircraft between the heights of 15 and 800 m and at different times of the day. The early morning profile at 06:23 UTC reveals drainage winds confined below the $\approx$200 m height in the lowest levels, and low wind speeds above. The next profile at
5 07:40 UTC shows low speeds at every altitude, suggesting a transition period between drainage and sea breeze regimes. Later in the day, the sea breeze develops and blows from the South-East at a speed of 5 ms^{-1} below a height of 400 m by 11:47 UTC, increasing to 7 ms^{-1} by 13:03 UTC. In addition, these last two profiles reveal that the breeze cell becomes confined below the 400 m height.

10 These different stages of wind reversals are captured by the model, as the comparison in Fig. 5 shows. At 06:30 UTC, the model underestimates the drainage wind intensity in the lowermost layers, while aloft there is some overestimation. At 07:50 UTC, the model reproduces the decrease in wind speed due to the transition between drainage and breeze regimes, still with a small over-prediction aloft. At 11:50 UTC
15 and 13:10 UTC, the model simulates a well-developed and persistent breeze (see also Fig. 6) consistent with the aircraft measurements. It is also worth noting that the wind shear observed for these last two profiles above $\approx$400 m is well-captured by the model.

5.3 3-D structure of simulated wind, pressure and turbulence

The previous two sections have shown that the model is able to solve, both realistically
20 and coherently with the observations, the mesoscale processes driven by heating and gravity during the campaign. This allows us to use the model as a "smart interpolator" to extrapolate point-wise observations and help untangle the 3-D character of the complex terrain circulations.

Figure 6 shows the evolution of horizontal streamlines and pressure fields on 2 July.
25 During the night, the drainage winds follow the direction of each valley (Fig. 6a). Vertical cross-sections at constant latitude between the height of 0 and 3000m show the thickness and extension of this drainage flow, which penetrates over the sea (Fig. 7a). After dawn, at 08:00 UTC, heating of the slopes oriented toward the sun allows the

development of up-slope winds, while in some areas close to the coast, nocturnal drainage persists (Fig. 6b). The gray lines in Fig. 6b show that there are some well-defined convergence zones of horizontal winds where vertical injection occurs. In these convergence zones, the vertical winds indicate positive vertical transport and upward advection of TKE at 39.45N, −0.87W (Fig. 7b). At the same time, there is a divergence zone at 39.45N,−0.63W, where the vertical wind is negative in the lower 200 m and sinking of TKE can be observed (Fig. 7b). Higher than 400 m above the sea, the wind coming from the East is connected to the up-valley injection. The return flow can be observed above 1200 m. A similar divergence center is found in the southern Jucar valley, 38.95N,−0.48W, surrounded by convergence lines (Fig. 6b). The horizontal gradient of the Sea Level Pressure is small at this stage of the morning. Thus, this situation shows a complex pattern of horizontal and vertical winds at this time of the day, when the scales of the processes are related to each valley size.

At 11:00 UTC, the valley breezes have merged into a combined breeze extending from the sea (where horizontal wind divergence is observed) to an inland convergence line located over the main mountain range parallel to the coast (Figs. 6c and 7c). The vertical injection shown at this time is stronger than before, reaching above the 2000 m height (Fig. 7c). The breeze cell confined to the first 400 m in Fig. 5 connects the coast with the mountain convergence and its return aloft. The cross-section parallel to the coast shows how the compensatory subsidence in the center of the valley limits the vertical mixing to the lower 300 m of the atmosphere. There is a continuous Sea Level Pressure gradient of 1–2 hPa within 60 km with a decrease from the coast to the interior.

At 15:00 UTC, the wind veers to the South-East over the sea, while inland, some changes in the position of the mountain convergence lines are observed (Fig. 6d). The negative pressure gradient between the center of the Jucar and Turia valleys and the coast is higher at this time, showing a decrease of more than 3 hPa in less than 60 km in the Jucar valley. Three hours later, at 18:00 UTC, while the wind direction over the sea continues to come from the South-East, the wind inland has changed to

North-East in the southern basin and to South-East in the northern basin (Fig. 6e). The development of this circulation at this time compensates for some of the spatial pressure gradients developed in previous hours between coastal sites and XA. Finally, at 21:00 UTC, the cooling of the surface air starts to organize drainage winds towards
5   the sea, while part of the flow shows some memory of the previous processes (Fig. 6f). The spatial variability of the pressure is now lower than during the evening, except in the higher north-east valleys.

6   Statistical assessment of the atmospheric model performances

The ability of the RAMS atmospheric model set-up to reproduce the main features of
10 the mesoscale circulations over the complex terrain of the Valencia region deserves a further, quantitative assessment. Table 2 gives a detailed statistical comparison between the observed and modeled temperatures, relative humidity and winds.
    Hourly outputs of the model during 1–2 July were spatially interpolated to the location of each station to calculate various model-data comparisons. We calculated the Mean
15 Error (ME) and the Root Mean Square Error (RMSE) for temperature and humidity. For winds, we calculated the RMSE of the Vector Wind Difference (VWD) defined in the Table 2 caption. This latter statistic, introduced by Stauffer and Seaman (1990) to evaluate the skill of their mesoscale assimilation system, has the main advantage of taking into account both wind speed and direction errors, which is very important
20 in the presence of wind reversals. In addition, we also calculated the wind speed Index Of Agreement (IOA), a measure of the degree to which a model's prediction is free of error (Willmott, 1981). The value of the IOA varies between 0 and 1, where 1 indicates perfect agreement and 0 complete disagreement between model and data. In Table 2, the seven meteorological stations are grouped into a coastal group (PO, CA,
25 SA, RI) and an inland group (AL, XA, VI) while the statistical comparison is performed separately during day and night.

6.1 Temperature and humidity

For temperature, the model-data RMSE for all stations is 1.49°C, with a ME of 0.04°C (i.e., no bias). The model performances for temperature are, in fact, very good if one compares the small value of the model-data misfit (Table 2) with either the large diurnal
[5] cycle amplitude of 15°C (Fig. 3) or the coast vs. inland temperature gradients of 4°C. When only the coastal stations are considered, the model shows no bias (ME = 0.03°C) and equally as good performances for both daytime and night time. For inland stations, the model has a slight negative bias during the day (ME = –0.24°C) and a slight positive one during the night (ME = 0.81°C). However, this overestimate of the diurnal temper-
[10] ature cycle does not degrade the model-data comparison, the RMSE values for the inland stations being similar to those of the coastal sites. For relative humidity, the value of the ME for the seven stations is very small (0.39%), indicating no systematic drier or wetter bias of the model. The model reproduces the RH variations well, as illustrated by an RMSE value of 18.09%. When grouping the stations into coastal and
[15] inland families, one can see from Table 2 that the model is slightly too dry on the coast (ME = –12.17%) and too wet inland (ME = +8.76%). The dry bias of the model for coastal stations is more pronounced during the night than during the day, while the wet bias for inland stations remains stable. The RMSE values are rather large (see also Fig. 3), and for coastal and inland stations, or during day and night, the RMSE seems
[20] to correlate with the model bias. Overall, the model performances for humidity are not as good as they were for temperature, as seen when comparing RMSE values to the mean gradients of humidity in the domain (not shown). Given that humidity depends on soil moisture availability, this result could indicate some shortcomings in the calculation of the soil moisture fields from the meteorological conditions of the previous months
[25] (Sect. 3).

The meteorological data collected aloft during the flights make it possible to complete the surface validation. For the horizontal transects, at 25m above ground, the model appears too warm (ME = 1.24°C), but at 50 m above ground, it is in excellent agreement

Title Page

Abstract	Introduction
Conclusions	References
Tables	Figures

◄   ►│

◄   ►

Back   Close

Full Screen / Esc

Printer-friendly Version

Interactive Discussion

with the data, except for mid-day (see Table 2). For the vertical profiles between 50 m and 800 m, the model matches the data well, although it is slightly too cool, with a maximum cold bias at mid-day (ME = −1.16°C). The RMSE is correlated with the model bias for all four profiles, underlining a persistent difference between the modeled and the observed temperatures. We found that the model performances for humidity mirror those for temperature when comparing the 25 m and 50 m levels. The model is too dry at 25 m but realistic at 50 m, and it differs from the data less during the stable regime in the early morning than at midday when convection occurs. Vertical profiles of humidity up to 800 m show that the model is in excellent agreement with the data (ME < 7%), but a more detailed inspection of the statistics reported in Table 2 suggests a slight dry bias during the early morning and a slight wet bias by midday. Higher values of RMSE than ME show that these positive or negative humidity biases are not systematic for all altitudes. The dry and warm bias of the model at 25 m could be due to the fact that rice fields were flooded during the campaign, which is not considered in the model. Such a likely underestimation of surface latent heat emissions has evidently more impacts at 25 m than at 50 m in the early morning, and later on contaminates the 50 m level by around midday through convective mixing, exactly as suggested by the model-data comparison in Table 2.

6.2 Wind

For wind speed, the model shows a slight positive bias (ME = 0.36 ms^{-1}). Averaged for all the stations, we have typical nocturnal values of ≈ 1 ms^{-1}, and daytime values of 6 ms^{-1}, giving an amplitude ≈ 5 ms^{-1} (see Fig. 3). The simulated wind has an RMSE of 1.54 ms^{-1}, which suggests good model performances, considering the amplitude of the signal. The wind speed IOA is 0.79, which is good, given the complexity of the mesoscale flow and the fact that the seven stations are representative of contrasted wind regimes inside the Valencia basin. The modeled wind speed at the coastal stations is accurate (ME = 0.04), but at the inland stations it is overestimated (ME = 0.79 ms^{-1}). In both cases, the mean bias remains lower than the RMSE. At

Mesoscale circulations over complex terrain: meteorology

G. Pérez-Landa et al.

inland sites, the wind speed RMSE is similar between day and night (Table 2). Despite this, considering that the magnitude of the wind speed is about four times lower during the night, it seems that the model shows worse skills at night than during the day. At coastal sites, a positive bias is found during the day (ME = +0.36m s^{-1}), and

a negative one (ME = –0.56) during the night. Also, at the coastal stations, the model performances are worse during the night, given the low prevailing winds. Overall, during the night, the model is found to be too windy inland and not windy enough on the coast. The inland stations are located up-valley on slopes whereas the coastal stations are on flat terrain. It seems here that the RAMS parameterization of the stable regime of the nocturnal PBL, controlling the drainage winds, does not reproduce the high spatial variability of the wind in the area.

For all stations the average VWD varies between 1.2 and 2.5 ms^{-1} during the campaign, up until the evening of 2 July, when it peaks at 4 ms^{-1} (Fig. 8). It is clear from Fig. 8 that the model simulates the wind vector worse for inland sites (VWD = 7 ms^{-1}) than for the coast, which can be explained by the fact that these stations are located close to the mountain convergence lines at the evening transition period of 2 July. A small deviation in the simulated location of the convergence line will have a strong impact in the VWD score (see Fig. 6e). For the coastal sites, the RMSE-VWD maximum ($\approx$4 ms^{-1}) occurs at 20:00 UTC and probably corresponds to the period of transition from the evening combined breeze circulation to the nocturnal drainage regime. A small bias in the timing of the wind speed drop could explain a degraded model-data agreement. Except for evening transition processes on 2 July, the VWD values vary between 1 and 3 ms^{-1} with no differences between coastal and inland locations. Minimum values around 1 ms^{-1} are observed at the times when the wind speed is weaker, during the transition period in the night of 1 July and the morning of 2 July.

The comparison between simulated and observed winds at the 25 and 50m heights shows that the model slightly underestimates wind at both heights and at all six transects. Bias values are quite similar although, taking into account the lower magnitude of the wind during the early morning, the skills are worse at this time. RMSE errors

|◄ | ►|

◄ | ►

Back | Close

Full Screen / Esc

Printer-friendly Version

Interactive Discussion

are correlated with ME and confirm the tendency to underestimate wind speed. The VWD parameter shows similar values to the RMSE, except at midday when higher values (especially the transect 11:59/12:22) indicate a deviation in the wind direction. Figure 4b shows this deviation. The wind profile statistics show the same features described in Sect. 5: overestimation in the early morning and small underestimation at midday. VWD and RMSE are similar in the first two profiles, indicating that the differences in wind speed are responsible for these biases. However, at midday, VWD are almost twice the RMSE, indicating differences in direction, as discussed in the previous section. It is clear that the results at 13:03 UTC are better that at 11:47 UTC. At any rate, considering the complex sheared wind profiles observed (Fig. 5), the model simulates this field reasonably well.

Overall, this statistical comparison shows that our RAMS set-up over the Valencia basin is capable of simulating mesoscale meteorology to a degree comparable to that of recent mesoscale modeling studies under weak synoptic conditions in complex terrain (Seaman and Michelson, 2000; Hanna and Yang 2001; Zhong and Fast 2003).

7 Discussion

The meteorological patterns of the two-day campaign are representative of typical summer conditions around the Mediterranean basin. We now summarize to what degreee the model provides realistic results in terms of the processes involved at the different stages of the mesoscale-circulations diurnal cycle, which controls tracer dispersion over the Valencia basin.

The main processes and spatial flow patterns during the nocturnal regime are simulated with high accuracy, although the comparison with station observations shows some discrepancies (Fig. 3). The station time series and airborne near-surface data indicate a tendency to over-predict the surface wind speed inland and under-predict it on the coast. In addition, the early morning vertical profiles near the coast also indicate that the wind speed aloft is overestimated. Model-data discrepancies are also

observed for the wind direction at the confluence of the different valleys. These short-comings may reflect inappropriate parameterizations of the stable boundary layers over complex terrain (Zhong and Fast 2003). We would also add the utmost importance of resolving topography at the highest possible resolution to capture drainage effects.

After dawn, our model is able to reproduce the local response of the flow to the surface heating differences at most sites, showing a complex wind field still strongly related to orography at the valley scale (e.g. Fig. 6b). The morning simulated wind flow shows realistic structures with local circulations configured in cells with convergence lines around each inland valley, while in the valleys open to the sea, the up-slope winds couple with the developing sea breeze and feed the flow directed towards the inland convergence lines. Positive and negative simulated vertical wind speeds develop in the convergence lines and over the center of divergence respectively, a process creating a three-dimensional flow structure. The sea breeze front progressively incorporates these circulatory cells as it penetrates deeper inland, homogenizing the flow. Such an interaction between thermally driven smaller scales in the early stages of mesoscale circulation development, has also been documented in other regions on the Spanish eastern coast (Millán et al., 1998).

At around midday, when the combined breeze is extending from the coast to the main mountain range, the model simulates a strong vertical injection of air at the convergence lines and a simultaneous sinking over the sea due to compensatory subsidence, in accordance with former studies (Millán et al., 1996). This chimney of ascending air plays a fundamental role in the transport of surface-emitted tracers, such as CO_2 (see companion paper). Both the observed and simulated wind vertical profiles indicate a strong shear over the coastal plains, where the combined breeze circulation is confined in the lowermost 400 m, a situation which can be called typical of summertime conditions in the region see also Galmarini et al. (2000). The time evolution of the combined breeze structure in the early afternoon is related to "self-organization" at the local scale, but it also participates in a larger coherent flow at the scale of the Iberian Peninsula and WMB. Our model results suggest that the changes both in the position

Mesoscale circulations over complex terrain: meteorology

G. Pérez-Landa et al.

of the convergence lines and in the horizontal wind patterns may be partly due to interactions with these latter two large scales. For instance, the South-easterly evening winds simulated over the sea could be due to the diurnal anti-cyclonic subsidence and veering of the flow usually occurring over the whole WMB at that time (Gangoiti et al., 2001).

In the evening when the solar warming diminishes, the mesoscale circulations have distributed the heat during their development over the whole Iberian Peninsula, and spatial gradients in surface temperature (and consequently in pressure) can be strong enough to affect the flow pattern. This effect of the ITL development is responsible for the evening increase in wind speed documented in the North of the Valencia basin by Millán et al. (1992). The wind changes observed on 2 July at the three sites analyzed seem to be a consequence of the same effect. The strong heating of the southern part of the Valencia basin induces a local decrease in pressure on 2 July, enabling the development of a North-east shift in the wind pattern after 18:00 UTC (Fig. 6e). We found that the model is able to reproduce both the heating and the corresponding wind changes at the stations, except for the wind direction change at Xativa (XA in Fig. 3d), a misfit that we attribute to a small southward bias in the modeled position of the convergence line (see Figs. 3d, f and 6e). In the evening and during the following night, in the absence of solar forcing, the thermal circulations decrease, favoring the development of the nocturnal regime and starting a new cycle.

The temporal and spatial evolution of the distinct meteorological processes as described above leaves an imprint on the statistical analysis of the model performances. The different scores between day and night and between coastal and inland stations show that the model has its "preferences". Namely, we find a generally excellent agreement with the observations when the diurnal wind regime is established, whereas during the transition periods when the temporal variability of the meteorological variables is higher, we witness degraded performances. Importantly, the evening veers in the flow when circulations are influenced by the horizontal pressure gradient can be resolved in the model, thanks to the nesting of several domains covering the phenomenon at all

EGU

scales. At face value, a larger spatial and temporal variability penalizes the model's sta-
tistical scores at that time of the day. Finally, the model is able to reproduce correctly the
terrain- dependent drainage winds during nocturnal stable conditions, although some
deficiencies persist in simulating this process, as reflected by positive and negative

5 biases in wind speed. During the night and early morning, the complex structure of
the terrain strongly determines the near-surface flow, thus ensuring better simulation
scores for surface stations than aloft. A high model resolution for resolving the main
valleys and mountain ranges is essential here for reproducing the katabatic flows.

8   Conclusions

10 Measurements collected during the RECAB summer campaign in the Valencia basin
are interpreted within a high-resolution set-up of the RAMS mesoscale model. This
allows us to describe and understand the complex sequence of non-stationary scenar-
ios, which are in constant transition and driven dynamically by the development of the
3-D wind-fields at local-to-regional scales. Aircraft and ground-based meteorological

15 measurements permit a quite detailed validation of the mesoscale simulations. As ex-
pected, the concatenated meteorological transitional processes have a marked diurnal
cycle. By means of measuring and modeling, we have been able to identify three main
(characteristic) patterns (and the corresponding transitions between them): 1) the noc-
turnal drainage flow regime with katabatic winds channeled by the valleys towards the

20 sea, 2) the combined breeze regime where the sea breeze merges with convective
uplift over the mountain ranges followed by a subsiding flow over the sea, and 3) the
evening regime, which, with a large enough pressure decrease, can interact with the
combined breeze and change the flow pattern. While the first two stages have been
documented to occur similarly in other East coast regions of Spain (Millán et al., 1996),

25 in the Valencia basin, the third stage (i.e., the evening change in pressure) may induce
a veering of the combined breeze to the North-east. These processes are represen-
tative of the typical conditions present in Valencia region at least six months per year

(see Appendix A).

We have carefully evaluated the RAMS model simulation for each regime and found that the model results are in good agreement with the data, with statistical scores comparable to those of other similar simulation studies (Seaman and Michelson, 2000; Hanna and Yang 2001; Zhong and Fast 2003). In terms of the model's ability solving processes, similar skills to other studies in complex terrain were found (Zhong and Fast 2003; De Wekker et al., 2005). The keys to the good performance of the model are: a resolution high enough to resolve the drainage flow, a proper initialization of soil moisture from a long enough spin-up carried out with improved lower boundary conditions through Land Use databases or satellite-processed SST, and the nesting of the high resolution model into a suite of domains that allow us to solve both the mesoscale processes at their corresponding scale and their interactions with the smaller scales in the Valencia region.

The nocturnal regime is perhaps the least properly captured. On the other hand, the simulation of the confined midday breeze cell represents the best performance of the model. At midday, we have found that the vertical profile information, in particular the height of the breeze cell and the intensity of the return flow, is the key to evaluating the model. All this should be borne in mind when dealing with the transport of CO_2 using the same wind fields (see companion paper).

In general, it is well known that landscape and terrain heterogeneities can induce spatially varying surface turbulent fluxes resulting in heterogeneous boundary layers (Pielke, 2002). Our study area combines the effects of land-sea contrasts, mountainous terrain and larger-scale mesoscale circulations. Therefore, not surprisingly, the lower-atmosphere properties that we have found are typical of the Thermal Internal Boundary Layer (TIBL) (Galmarini et al., 2000). The measurements available during the campaign allowed us to characterize some of the properties of such a TIBL during breeze development, although vertical profiles to a higher altitude and further inland would have been very useful as well. It is very encouraging that, despite the inherent complexity of the system studied, the RAMS model could reproduce faithfully the

main flow patterns. However, it is important to keep in mind that turbulence parameterizations of mesoscale models are derived from theories and data for horizontally homogeneous steady-state boundary layers (Pielke, 2002). Thus, it is likely that the simulated turbulence fields (usually provided for dispersion models) could have been
conditioned by this limitation. New data over complex terrain could be useful to test the mesoscale models beyond their range of normal applicability, with the aim of eventually improving them.

Appendix A   Temporal representativity of the case study

2 July can be considered representative of typical summer meteorological conditions on the Spanish Mediterranean coasts as the main synoptic-scale features (Fig. A1) are in agreement with the mean meteorological conditions in the region during the early summer (Fig. 2). Both synoptic charts reflect a high pressure system dominating the center of the Atlantic ocean and Northern Europe, a Thermal Low on the Iberian Peninsula and another high pressure region over the Western Mediterranean, favoring the development of mesoscale circulations.

Some of the wind field features diagnosed in this paper for 2 July seems to be present in the basin at least during half of the year. Thus, "time roses" for the selected stations (VI, XA and SA), representing the time frequencies in which the wind blows from a specified direction and covering April to September from 2001 to 2005, show the existence of "wings" in markedly different directions (Fig. A2). This characteristic indicates that the dominant winds from the coast inland are affected by channeling and by diurnal cycles: nocturnal drainage winds towards the sea and diurnal thermal circulations towards inland.

From a statistical point of view, it is interesting to note how the wind direction shifts towards NE at the SA station during the late afternoon. In a parallel way, the XA station also shows a wind shifting during the same diurnal period, although due to the change in relative position to the mountains; in this case wind shifting is monitored towards

NNE. This diurnal feature was described in detail for the case study analyzed in this paper.

During nighttime, these two stations show drainage winds flowing towards the sea and channeled by the orographic features. It is statistically significant to note how the SA station shows two predominant drainage directions, the WNW flows draining down from the Turia valley and the the WWS flows linked to the Jucar valley (as was described for the case study presented in this paper). Further inland, the wind field measured at the VI station is subjected to topographic channeling of both diurnal and nocturnal flows.

References

Anderson, J. R., Hardy, E. E., Roach, J. T., and Witmer, R. E.: A land use and land cover classification system for use with remote sensor data, U.S. Geological Survey Professional Paper 964, Government Printing Office, Washington D.C., Available on-line http://landcover.usgs.gov/pdf/anderson.pdf, 1976.

Attane, I. and Courbage, Y : Demography in the Mediterranean region. Plan Bleu. Paris, Economica. Available on-line http://www.planbleu.org/publications/demo_uk_part1.pdf, 2004.

Aubinet, M., Grelle, A., Ibrom,A., Rannik, U., Moncrieff, J., Foken, T., Kowalski, A. S., Martin, P. H., Berbigier, P., Bernhofer, C., Clement, R., Elbers, J., Granier, A., Grunwald, T., Morgenstern, K., Pilegaard, K., Rebmann, C., Snijders, W., Valentini, R., and Vesala, T.: Estimates of the annual net carbon and water exchange of European forests: the EUROFLUX methodology, Adv. Ecol. Res., 30, 113–175, 2000.

Badenas, C., Caselles, V., Estrela, M. J., and Marchuet R.: Some improvements on the processes to obtain accurate maps of sea surface temperature from AVHRR raw data transmitted in real time, Part 1. HRPT images, Int. J. Remote Sens., 18, 1743–1767, 1997.

Baklanov A., Batchvarova, E., Calmet, I., Clappier, A., Chordá, J. V., Diéguez, J. J., Dupont, S., Fay, B., Fragkou, E., Hamdi, R., Kitwiroon, N., Leroyer, S., Long, N., Mahura, A., Mestayer, P., Nielsen, N. W., Palau, J. L., Pérez-Landa, G., Penelon, T., Rantamäki, M., Schayes G., and Sokhi R. S.: Improved parameterisations of urban atmospheric sublayer and urban physiographic data classification, D4.1, 4.2 and 4.5 FUMAPEX Report, edited by Baklanov, A. and P. Mestayer, DMI, Denmark, DMI Scientific Report: #04-05, ISBN nr. 87-7478-506-0, 2004.

Bakwin, P. S., Tans, P. P., Hurst, D. F., and Zhao, C.: Measurements of carbon dioxide on very tall towers: Results of the NOAA/CMDL program, Tellus, 50B, 401–415, 1998.

Caplan, P., Derber, J., Gemmill, W., Hong, S. Y., Pan, H. L., and Parish, D.: Changes to the NCEP operational medium-range forecast model analysis/forecast system, Weat. Forecasting, 12, 581–594, 1997.

CEC (Commission of the European Communities): CORINE Land cover, Guide Technique, Brussels, Available on-line, http://reports.eea.eu.int/COR0-landcover/en, 1995.

Chang, Y. S., Carmichael, G. R., Kurita, H., and Ueda H.: The transport and formation of photochemical oxidants in Central Japan, Atmos. Environ., 23, 363–393, 1989.

Chen, C. and Cotton, W. R.: A one-dimensional simulation of the stratocumulus-capped mixed layer, Boundary-Layer Meteor., 25, 289–321, 1983.

Chevillard, A., Karstens, U., Ciais, P., Lafont, S., and Heimann, M.: Simulation of atmospheric CO_2 over Europe and Siberia using the regional scale model REMO, Tellus, 54B, 872–894, 2002.

Crawford, T. L., Dobosy, R. J., McMillen, R. T., Vogel, C. A., and Hicks, B. B.: Air-surface exchange measurement in heterogeneous regions: extending tower observations with spatial structure observed from small aircraft, Glob. Change Biol., 2, 275–285, 1996.

De Wekker, S. F. J., Steyn, D. G., Fast, J. D., Rotach, M. W., and Zhong S.: The performance of RAMS in representing the convective boundary layer structure in a very steep valley, Env. Fluid Mech. 5, 35–62, 2005.

Denning, A. S., Fung, I. Y., and Randall, D.: Latitudinal gradient of atmospheric CO_2 due to seasonal exchange with land biota, Nature, 376, 240–243, 1995.

Desjardins, R. L., MacPherson, J. I., Mahrt, L., et al.: Scaling up flux measurements for the bo-

real forest using aircraft tower combinations, J. Geophys. Res., 102, 29 125–29 134, 1997.

Desjardins, R. L., Brach, E. J., Alno, P., and Schuepp, P. H.: Aircraft monitoring of surface carbon dioxide exchange, Science, 216, 733–735, 1982.

Eastman, J. L., Coughenour, M. B., and Pielke, R. A.: The regional effects of CO_2 and land-
5 scape change using a coupled plant and meteorological model, Glob. Change Biol., 7, 797–815, 2001.

Galmarini, S. and Attié J. L.: Turbulent transport at the Thermal Internal Boundary-Layer top: Wavelet Analysis of Aircraft Measurements, Boundary-Layer Meteorol, 94, 175–196, 2000.

Gangoiti, G., Millán, M. M., Salvador, R., and Mantilla, E.: Long-range transport and re-
10 circulation of pollutants in the western Mediterranean, during the project Regional Cycles of Air Pollution in the West-Central Mediterranean Area, Atmos. Environ., 35, 6267–6276, 2001.

Georgiadis, T., Giovanelli, G, and Fortezza F.: Vertical layering of photochemical ozone during land-sea breeze transport, Il Nuovo Cimento, 17, 371–375, 1994.

15 Gioli, B., Miglietta, F., De Martino, B., Hutjes, R. W. A , Dolman, H. A. J., Lindroth, A., Schu-macher, M., Sanz, M. J., Manca, G., Peressotti, A., and Dumas, E. J.: Comparison between tower and aircraft-based eddy covariance fluxes in five European regions, Agric. For. Mete-orol., 127, 1–16, 2004.

Hanna, S. R. and Yang R.: Evaluations of mesoscale model simulations of near-surface winds,
20 temperature gradients, and mixing depths, J. Appl. Meteor. 40, 1095–1104, 2001.

Hutjes, R., van den Bulk, W. C. M., Cosin, S., et al.: Regional Assessment and monitoring of the carbon balance within Europe (RECAB), Final Report. Alterra, PO Box 47, 6700 AC, Wageningen, Netherlands, 2003.

Jacobson, M. Z.: Effects of soil moisture on temperatures, winds, and pollutant concentrations
25 in Los Angeles, J. Appl. Meteorol., 38, 607–616, 1999.

Kallos, G., Kotroni, V., Lagouvardos, K., and Papadopoulos, A.,: On the long-range transport of air pollutants from Europe to Africa, Geophys. Res. Lett., 25, 5, 619–622, 1998.

Lalas, D. P., Tombrou-Tsella, M., Petrakis, M., Asimakopoulos, D. N., and Helmis, C.: An exper-imental study of the horizontal and vertical distribution of ozone at Athens, Atmos. Environ.,
30 21, 2681–2693, 1987.

Lanicci, J. M., Carlson, T. N., and Warner, T. T.: Sensitivity of the Great Plains severe-storm environment to soil-moisture distribution, Mon. Wea. Rev., 115, 2660–2673, 1987.

Lu, R. and Turco, R. P.: Air pollutant transport in a coastal environment. Part I. Two-dimensional

Mesoscale circulations over complex terrain: meteorology

G. Pérez-Landa et al.

simulations of sea-breeze and mountain effects, J. Atmos. Sci., 51, 2285–2308, 1994.

Lu, L., Denning, A. S., da Silva-Dias, M. A., da Silva-Dias, P., Longo, M., Freitas, S. R., and Saatchi, S.: Mesoscale circulations and atmospheric CO_2 variations in the Tapajós Region, Pará, Brazil, J. Geophys. Res., 110, D21102, doi:10.1029/2004JD005757, 2005.

5 Mahfouf, J. F.: Analysis of Soil Moisture fron Near-Surface Parameters: A Feasibility Study, J. Appl. Meteor., 30, 1534–1547, 1991.

McKendry, I. G., Steyn, D. G., Lundgren, J., Hoff, R. M., Strapp, W., Anlauf, K., Froude, F., Martin, J. B., Banta, R. M., and Olivier, L. D.: Elevated ozone layers and vertical downmixing over the Lower Fraser Valley, BC, Atmos. Environ., 31, 2135–2146, 1997.

10 Mellor, G. L. and Yamada, T.: Development of a turbulence closure model for geophysical fluid problems, Rev. Geophys. and Space Phys., 20, 851–875, 1982.

Michener, W. K., Blood, E., R., Bildstein, K. L., Brinson, M. M., and Gardner, L. R.,: Climate change, hurricanes and tropical storms, and rising sea level in coastal wetlands, Ecol. Appl., 7, 3, 770–801, 1997.

15 Miglietta, F., Pereira, J., Sanz, M. J., Rambal, S., Seufert, G., Valentini, R., Liakatas, A., Rayement, M., Dolman, H., Berbigier, P., Ibrom, A., and Tenhunen, J.: Monitoring Carbon and water vapour fluxes in Mediterranean-type ecosystems: the results of the EU-Medeflu project, in: Challenges of a Changing Earth, Proceedings of the Global Change Open Science Conference, Amsterdam, The Netherlands, 10–13 July, 2001.

20 Millán, M. M., Alonso, L., Legarreta, J. A., Albizu, M. V., and Ureta I.: A fumigation episode in an industrialized estuary: Bilbao, November 1981, Atmos. Environ., 18, 563–572, 1984.

Millán, M. M., Artiñano, B., Alonso, L., Castro, M., Fernandez-Patier R., and Goberna, J.: Meso-Meteorological Cycles of Air Pollution in the Iberian Peninsula, (MECAPIP), Air Pollution Research Report 44, EUR No. 14834, European Commission DG XII/E-1, Rue de la Loi,

25 200, B-1040, Brussels, 1992.

Millán, M. M., Salvador, R., Mantilla, E., and Artiñano, B.: Meteorology and photochemical air pollution in Southern Europe: experimental results from EC research projects, Atmos. Environ., 30, 1909–1924, 1996.

Millán, M. M., Salvador, R., Mantilla, E., and Kallos, G.: Photooxidants dynamics in the Mediter-

30 ranean basin in summer: Results from European research projects, J. Geophys. Res., 102 (D7), 8811–8823, 1997.

Millán, M. M., Estrela, M. J., and Badenas, C.: Meteorological processes relevant to forest fire dynamics on the Spanish Mediterranean coast, J. Appl. Meteor., 37, 83–100, 1998.

Title Page

Abstract | Introduction

Conclusions | References

Tables | Figures

◄ | ►

◄ | ►

Back | Close

Full Screen / Esc

Printer-friendly Version

Interactive Discussion

Molinari, J.: A general form of Kuo cumulus parameterisation, Mon. Wea. Rev., 113, 1411–1416, 1985.

Moran, M. D. and Pielke, R. A.: Evaluation of a mesoscale atmospheric dispersion modeling system with observations from the 1980 Great Plains Mesoscale Tracer Field Experiment, Part I: Datasets and meteorological simulations, J. Appl. Meteor., 35, 281–307, 1996.

Mucher C. A., Steinnocher, K. T., Kressler, F. P., and Heunks, C.: Land cover characterisation and change detection for environmental monitoring of pan-Europe, Int. J. Remote Sens., 21 (6-7), 1159–1181, 2000.

Nicholls, M. E., Denning, A. S., Prihodko, L., Vidale, P. L., Davis, K., and Bakwin P.: A multiple-scale simulation of variations in atmospheric carbon dioxide using a coupled biosphere-atmospheric model, J. Geophys. Res., 109, D18117, doi:10.1029/2003JD004482, 2004.

Olivier, J. G. J. and Berdowski, J. J. M.: Global emissions sources and sinks, in: The Climate System, edited by: Berdowski, J., Guicherit, R., and Heij, B.J., A. A. Balkema Publishers/Swets & Zeitlinger Publishers, Lisse, The Netherlands, ISBN 90-5809-255-0, 33–78, 2001.

Ookouchi, Y., Segal, M., Kessler, R. C., and Pielke, R. A.: Evaluation of soil moisture effects on the generation and modification of mesoscale circulations, Mon. Wea. Rev., 112, 2281–2292, 1984.

Orciari, R., Georgiadis, T., Fortezza, F., Alberti, L., Leoncini, G., Venieri, L., Gnani, V., Montanari, T., and Rambelli, E.: Vertical evolution of photochemical ozone over greater Ravenna, Annali di Chimica, 88, 403–411, 1998.

Pérez-Landa, G., Palau, J. L., Mantilla, E., and Millán, M. M.: A study of the dispersion of an elevated plume on complex terrain under summer conditions, paper presented at 15th Symposium on Boundary Layers and Turbulence, American Meteorological Society, Wageningen, The Netherlands, 346–349, 2002.

Pielke, R. A., Cotton, W. R., Walco, R. L., Tremback, C. J., Lyons, W. A., Grasso, L. D., Nicholls, M. E., Moran, M. D., Wesley, D. A., Lee, T. J., and Copeland, J. H.: A comprehensive meteorological modelling system RAMS, Meteor. Atmos. Phys., 49, 69–91, 1992.

Pielke Sr., R. A.: Mesoscale meteorological modeling, 2nd Edition, Academic Press, San Diego, CA, 676 pp, 2002.

Reynolds, R. W. and Smith T. M.: Improved global sea surface temperature analyses using optimum interpolation, J. Climate, 7, 929–948, 1994.

Salvador, R., Millán, M. M., and Calbo, J.: Horizontal Grid Size Selection and its influence on

Mesoscale circulations over complex terrain: meteorology

G. Pérez-Landa et al.

Mesoscale Model Simulations. J. App. Met., 38, 1311–1329, 1999.

Seaman, N. L. and Michelson, S. A.,: Mesoscale meteorological structure of a high-ozone episode during the 1995 NARSTO-Northeast study. J. Appl. Meteor., 39 (3), 384–398, 2000.

Simmons, A. J. and Gibson, J. K.: The ERA 40 Project plan, ERA-40 Project Report Series N° 1, ECMWF, Reading, UK, 63pp, 2000.

Smith, C. B., Lakhtakia, M. N., Capehart, W. J., and Carlson, T. N.: Initialization of soil-water content in regional-scale atmospheric prediction models, Bull. Amer. Meteor. Soc., 75, 585–593, 1994.

Stauffer, D. R. and Seaman, N. L.: Use of Four-Dimensional Data Assimilation in a limited-area mesoscale model, Part I: Experiments with Synoptic-Scale Data. Mon. Wea. Rev., 6, 1250–1277, 1990.

Walko, R. L., Band, L. E., Baron, J., Kittel, T. G. F., Lammers, R., Lee, T. J., Ojima, D., Pielke Sr. R. A., Taylor, C., Tague, C., Tremback, C. J., and Vidale, P. J.: Coupled atmospheric-biophysics-hydrology models for environmental modeling, J. Appl. Met., 39, 931–944, 2000.

Walko, R. L., Cotton, W. R., Meyers, M. P., and Harrington J. Y.: New RAMS cloud microphysics parameterization. Part I: The single-moment scheme, Atmos. Res.,38, 29–62, 1995.

Willmott, C. J.: On the validation of models. Phys. Geog., 2, 184–194, 1981.

Wofsy, S. C., Harriss, R. C., and Kaplan, W. A.: Carbon dioxide in the atmosphere over the Amazon Basin, J. Geophys. Res., 93, 1377–1387, 1988.

Zhong, S. and Fast, J.: An evaluation of MM5, RAMS, and Meso ETA at sub-kilometer resolution using VTMX field campaign data in the Salt Lake Valley. Mon. Wea. Rev., 131, 1301–1322, 2003.

Ziomas, I. C., Gryning, S. E., and Borstein R. D. (Eds.): The Mediterranean campaign of photo-chemical tracers-transport and chemical evolution (MEDCAPHOT-TRACE): Athens, Greece 1994–1995, Atmos. Environ., 32, 2043–2326, 1998.

Table 1. Flights carried out on 2 July.

Time Interval (UTC)	Type	Coordinates	Height (m)
06:23-06:30	Profile	39.36N; 0.35W	15-800
07:40-07:45	Profile	39.37N; 0.35W	15-800
11:47-11:51	Profile	39.37N; 0.36W	15-800
13:03-13:08	Profile	39.36N; 0.36W	15-800
06:31-06:41	Hz. Transect	39.38N; 0.36W - 39.21N; 0.27W	50
06:43-06:53	Hz. Transect	39.21N; 0.27W - 39.38N; 0.36W	50
06:54-07:04	Hz. Transect	39.39N; 0.35W - 39.21N; 0.27W	50
07:05-07:15	Hz. Transect	39.21N; 0.27W - 39.38N; 0.36W	25
07:16-07:26	Hz. Transect	39.38N; 0.35W - 39.21N; 0.27W	25
07:27-07:38	Hz. Transect	39.21N; 0.27W - 39.39N; 0.36W	25
11:54-12:04	Hz. Transect	39.39N; 0.36W - 39.20N 0.27W	50
12:05-12:15	Hz. Transect	39.21N; 0.27W - 39.38N 0.35W	50
12:16-12:26	Hz. Transect	39.39N; 0.36W - 39.21N 0.27W	50
12:27-12:37	Hz. Transect	39.21N; 0.27W - 39.38N; 0.38W	25
12:39-12:49	Hz. Transect	39.39N; 0.35W - 39.21N; 0.27W	25
12:52-13:02	Hz. Transect	39.21N; 0.27W - 39.39N; 0.34W	25

Table 2. Model skills against surface and aircraft observations. The seven surface stations are grouped by location into Coastal (PO, CA, SA and RI) and Inland (AL, VI and XA). Observations aloft are grouped considering the trajectory and times of the flights. N represents the number of observations included in the calculation of Mean Error, Root Mean Square Error, Index of Agreement and Vector Wind Difference for the respective variables. P represents the simulated value and P_o observation, while M_o is the average observed wind speed for N values in the corresponding formulas:

$$ME = \frac{1}{N}\sum_{i=1}^{N}(P - P_o) \qquad IOA = 1 - \frac{N(RMSE)^2}{\sum_{i=1}^{N}(|P - M_o| + |P_o - M_o|)^2}$$

$$RMSE = \sqrt{\frac{1}{N}\sum_{i=1}^{N}(P - P_o)^2} \qquad VWD = \sqrt{(u - u_o)^2 + (v - v_o)^2}$$

|		Wind vector (ms^{-1})					Temp. (°C)			Rel. Hum. (%)		
		ME	RMSE	IOA	VWD	N	ME	RMSE	N	ME	RMSE	N
Surface Stations (1 – 2 July)												
All Stations	All	0.36	1.54	0.79	2.18	300	0.04	1.49	300	0.39	18.09	215
	Day	0.52	1.43	0.84	2.28	195	-0.15	1.48	195	2.07	17.72	140
	Night	0.07	1.72	0.61	1.99	105	0.38	1.51	105	-2.76	18.75	75
Coastal Stations	All	0.04	1.47	0.78	2.04	171	-0.03	1.43	171	-12.17	20.42	86
	Day	0.36	1.21	0.86	2.11	111	-0.08	1.31	111	-9.37	20.22	56
	Night	-0.56	1.86	0.63	1.93	60	0.06	1.63	60	-17.41	20.77	30
Inland Stations	All	0.79	1.63	0.80	2.36	129	0.13	1.56	129	8.76	16.35	129
	Day	0.73	1.69	0.84	2.51	84	-0.24	1.67	84	9.70	15.84	84
	Night	0.92	1.51	0.59	2.07	45	0.81	1.34	45	7.00	17.27	45
Horizontal Transects (2 July)												
07:09-07:32	25 m	-0.75	0.92	-	1.11	62	1.24	1.42	62	-9.66	10.29	62
12:32-12:55	25 m	-0.88	1.17	-	1.87	65	2.14	2.35	65	-13.98	15.18	65
06:36-06:59	50 m	-0.73	1.17	-	1.47	63	0.09	0.74	63	0.32	5.76	63
11:59-12:22	50 m	-0.37	0.84	-	2.49	62	0.83	1.06	62	-7.09	8.75	62
Vertical Profiles (2 July)												
06:23	15-800m	2.26	3.42	-	3.44	14	-0.36	0.65	14	-4.66	13.10	14
07:40	15-800m	1.23	1.51	-	1.95	14	-0.21	0.62	14	-5.33	14.18	14
11:47	15-800m	-1.99	2.46	-	4.27	14	-1.16	1.69	14	6.83	14.18	14
13:03	15-800m	-0.20	2.05	-	3.56	14	-0.75	0.95	14	4.65	8.88	14
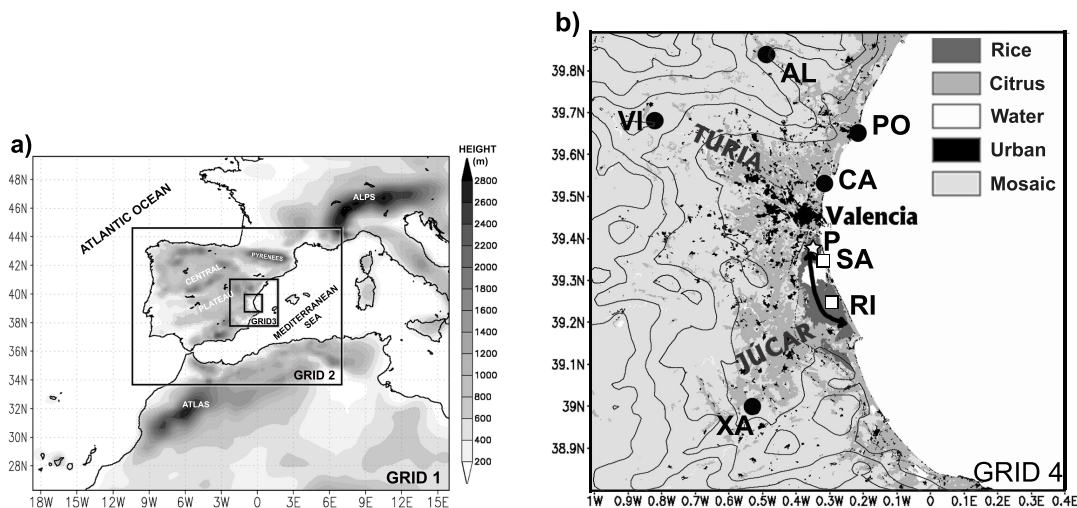
Fig. 1. **(a)** Domain configuration and orography of the RAMS model showing the four nested domains of increasing horizontal resolution. The largest domain (GRID 1) has a grid length of 40.5 km and the smallest (GRID 4), of 1.5 km. **(b)** Characteristics of the smallest-domain simulated meteorology is compared to the campaign measurements. Black lines show the orography every 200 m. Grey-scaled colors show the different land cover types (see legend). The location of the meteorological stations (black circles), eddy-covariance flux towers (open squares), airborne horizontal transect (black arrow) and vertical profiles (stars) can be seen.

Title Page

Abstract | Introduction

Conclusions | References

Tables | Figures

◄◄ | ►►

◄ | ►

Back | Close

Full Screen / Esc

Printer-friendly Version

Interactive Discussion

EGU

G. Pérez-Landa et al.

a) June 2001 Averaged Sea Level Preassure and Temperature from ECMWF
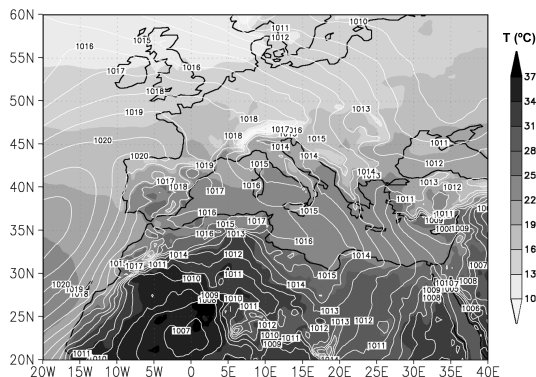
b) June 2001 Averaged Diurnal Cycle of Pressure from ECMWF
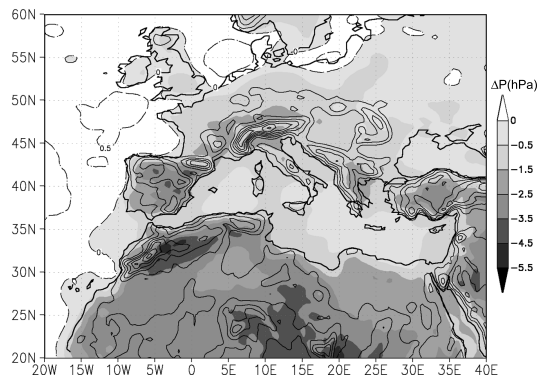
Fig. 2. (a) Average Sea Level Pressure (white contour lines) and 2m Temperature (gray colors represent ˚C) in June 2001 from ECMWF weather reanalyses. **(b)** Average diurnal cycle of Sea Level Pressure in hPa, taken from the difference of ECMWF fields at 18:00 and 00:00 UTC, in shaded lines when negative and dashed contour lines when positive. Solid contour lines represent the model topography every 300 m. Note the correlation between the diurnal cycle of pressure and topography.

Title Page

Abstract | Introduction

Conclusions | References

Tables | Figures

◀ | ▶

◀ | ▶

Back | Close

Full Screen / Esc

Printer-friendly Version

Interactive Discussion
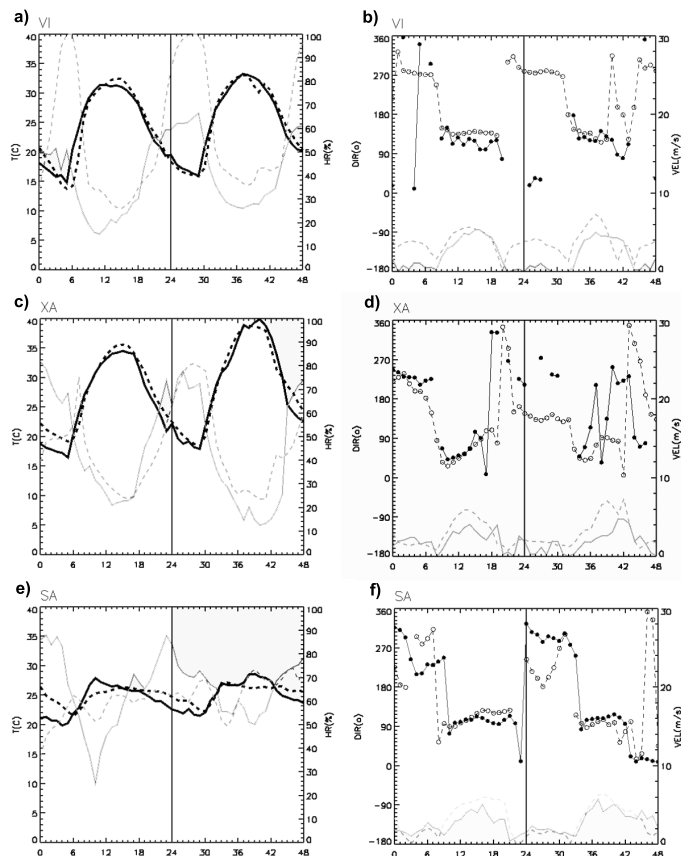
Fig. 3. Measured (continuous line) and simulated (discontinuous line) time series on 1 and 2 July 2001 in VI, XA and SA (see Fig. 1b). On the left: temperature (black) and relative-humidity (gray). On the right: wind speed (gray) and wind direction (black). When the observed or simulated wind speed was less or equal to $0.5\,\mathrm{ms}^{-1}$, the wind direction was not drawn.
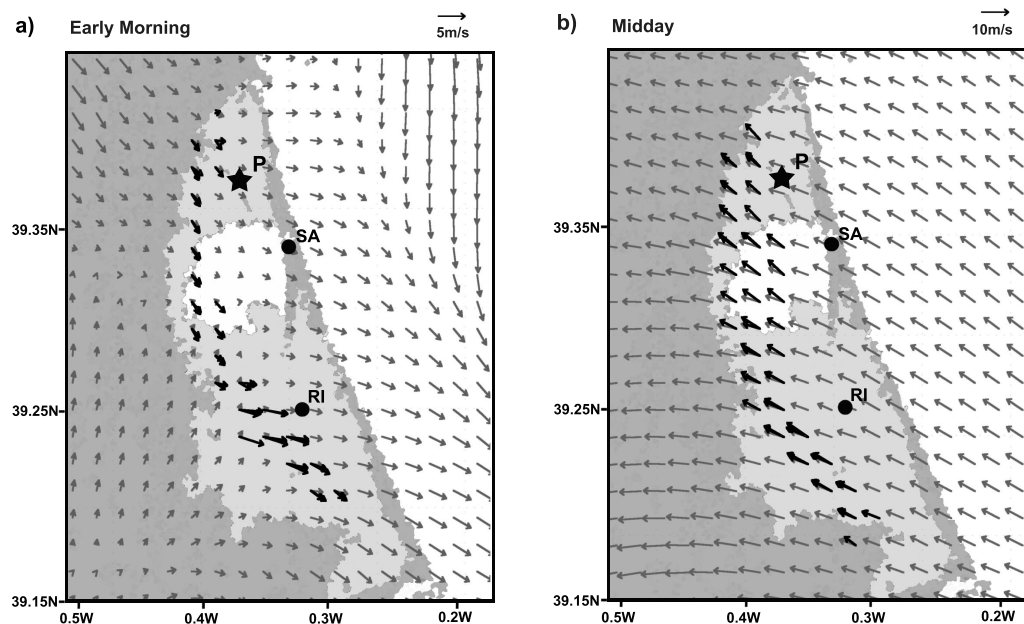
Fig. 4. (a) Early morning horizontal wind vectors at 50 m above ground. Thick black arrows: observed winds during the airborne transects at 06:50 UTC on 2 July. Thin gray arrows: modeled winds at the same time. Grey regions correspond to the same land cover types as in Fig. 1. **(b)** Same fields but for midday conditions, at 12:10 UTC. Note that corresponding wind scales are drawn at the top right of each panel.
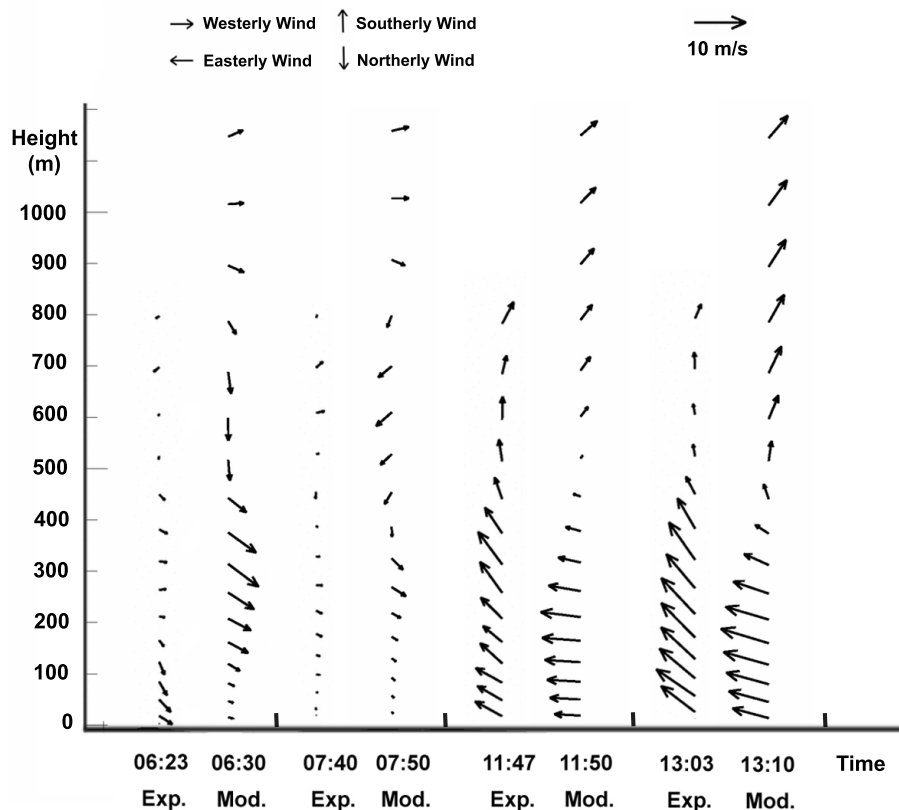
Fig. 5. Experimental (left) and modeled (right) vertical profiles of horizontal winds over the rice paddy fields at the aircraft campaign location (marked with P in Fig. 1b) at different times on 2 July.

Title Page

Abstract | Introduction

Conclusions | References

Tables | Figures

◀ | ▶

◀ | ▶

Back | Close

Full Screen / Esc

Printer-friendly Version

Interactive Discussion

EGU
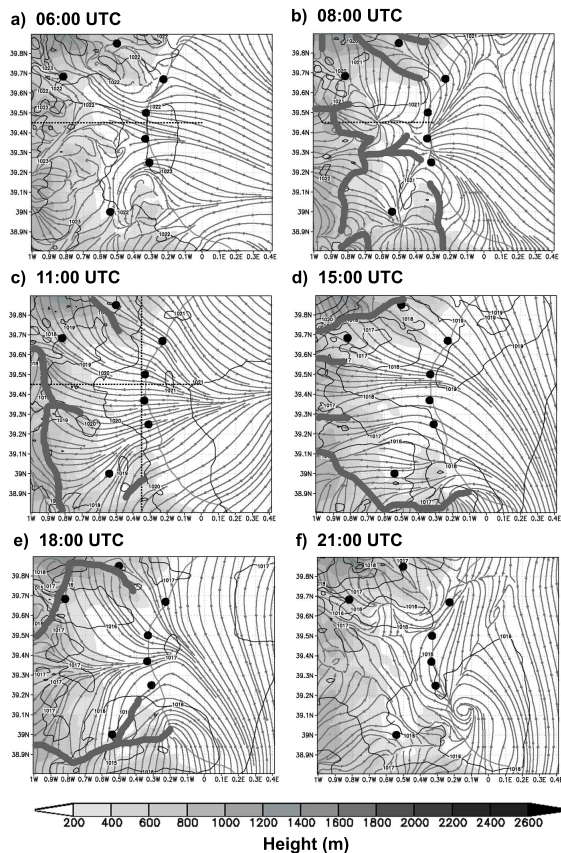
Fig. 6. Horizontal streamlines and Sea Level Pressure simulations near the surface (at ≈15 m) at different intervals on 2 July: **(a)** at 06:00, **(b)** at 08:00 UTC, **(c)** at 11:00 UTC, **(d)** at 15:00 UTC, **(e)** at 18:00 UTC, and **(f)** at 21:00. The thick gray solid lines represent convergence lines of the horizontal wind. The black dotted lines indicate the location of the cross-sections drawn in Fig. 7. Closed circles represent the location of ground stations (Fig. 1b).
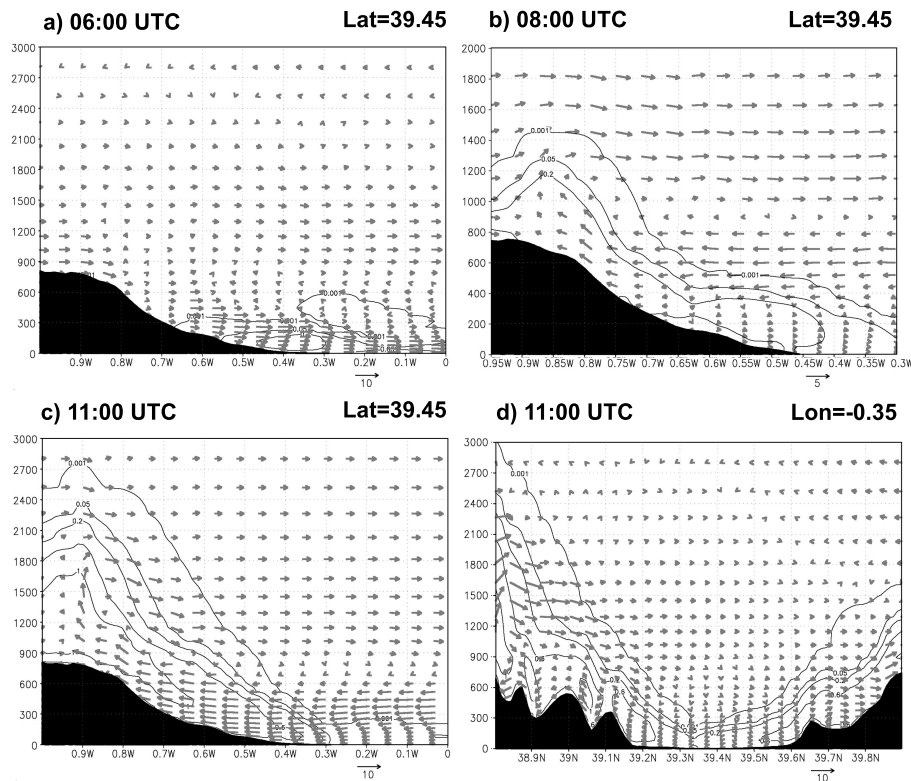
Fig. 7. Vertical cross-sections of simulated TKE (m^2s^{-2}) and wind (ms^{-1}). Contour lines represent TKE and vectors represent the wind component projected in the direction of the cross-section and with the vertical wind multiplied by 10. Each plot corresponds to the cross-sections drawn in Fig. 6 at constant latitude at the respective times, except for case **(d)** which represents a cross-section at constant longitude at 11:00 according to Fig. 6c. Note the different wind scaling and maximum height in **(b).**
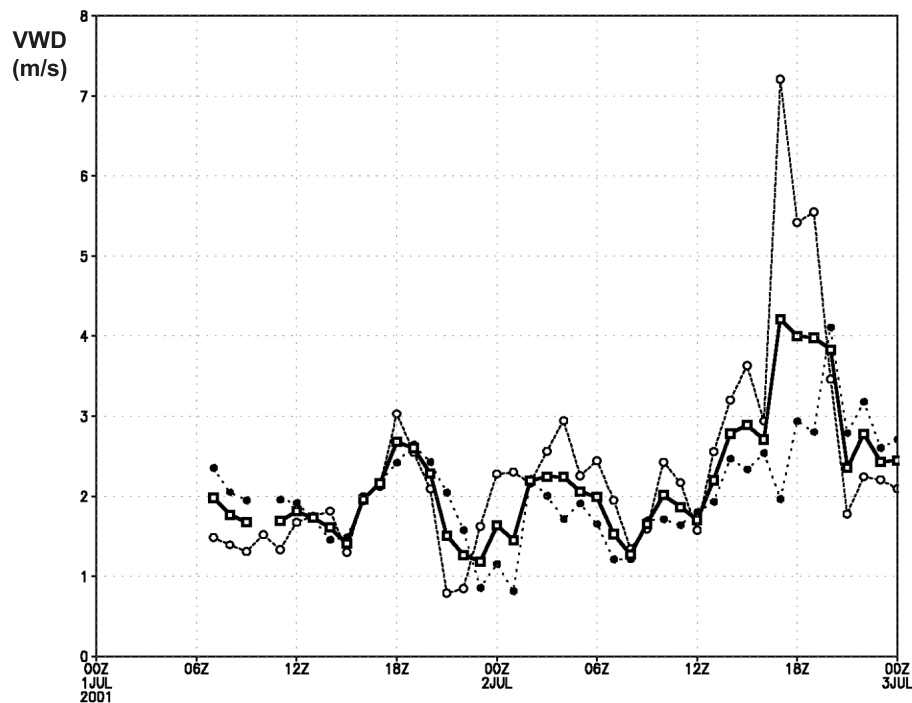
Fig. 8. Time series of VWD averaged for the seven surface stations (Solid) and grouped by location into Coast: PO, CA, SA and RI (dots) and Inland: AL, VI and XA (dashed).

Mesoscale circulations over complex terrain: meteorology

G. Pérez-Landa et al.

1000hPa Sea Level Pressure, Temperature 1200 UTC 2nd July 2005
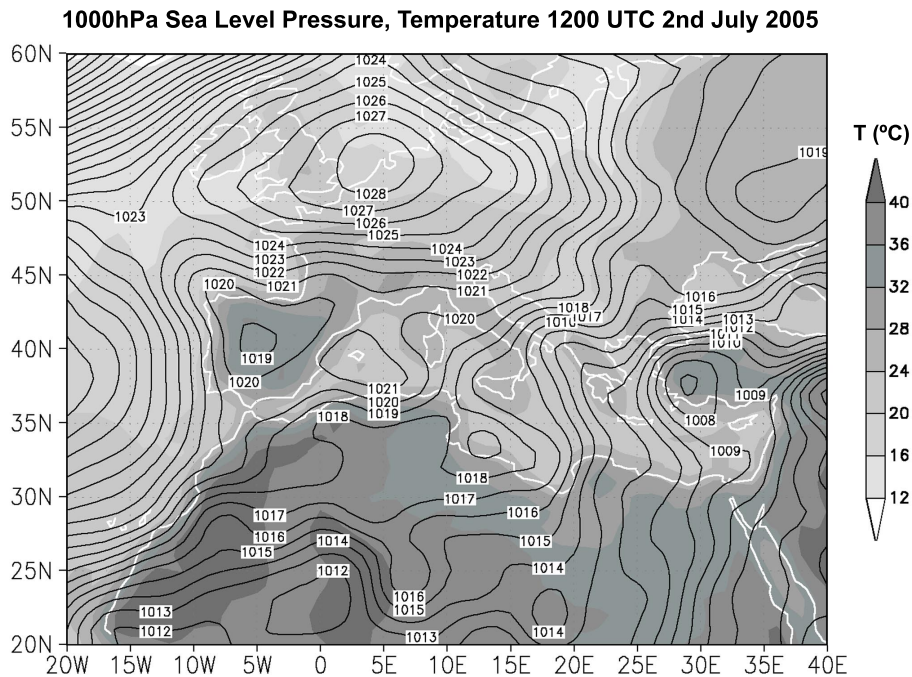
Fig. A1. Temperature (°C) at 1000 hPa and Sea Level Pressure (hPa) fields from the AVN global model at 1200 UTC on 2 July.
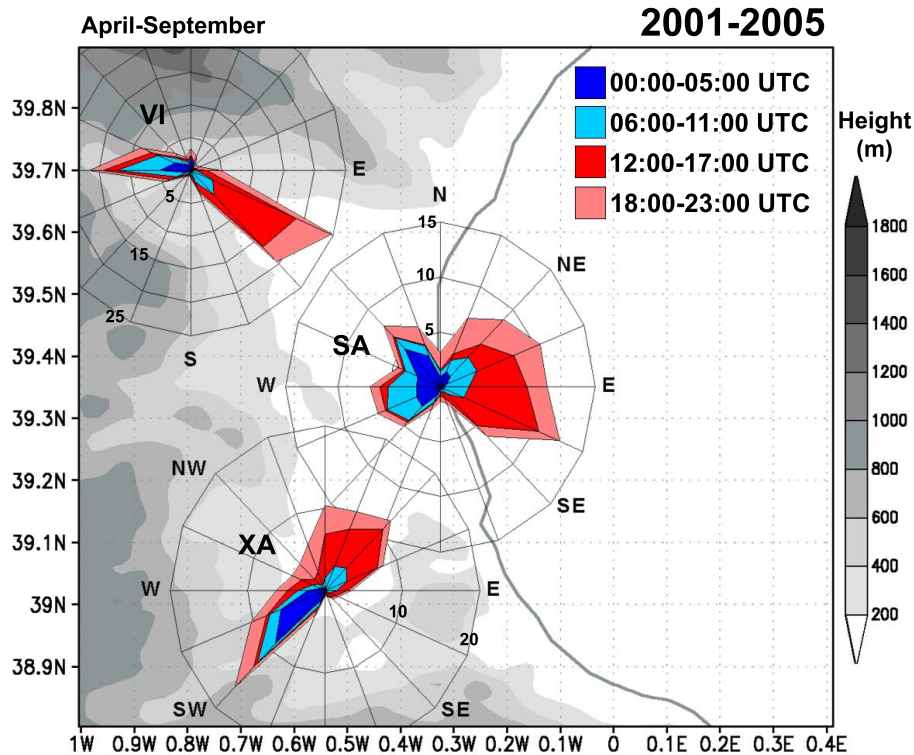
Fig. A2. "Time rose" in VI, XA and SA from April to September for five years (2001–2005). Wind speed intervals from usual "wind roses" have been replaced by the time intervals shown in the legend. This shows the prevalent directions on each site during the diurnal cycle. The "time roses" are drawn at their respective locations over the model high-resolution topography with the scale in %.

Title Page

Abstract | Introduction

Conclusions | References

Tables | Figures

◄ | ►

Back | Close

Full Screen / Esc

Printer-friendly Version

Interactive Discussion